Sequential pore wall functionalization in covalent organic frameworks and application to stable camptothecin delivery systems

Artur De Santana Oliveira[a, b], Eva María Rivero-Buceta[a], Carla Vidaurre-Agut[a,c], Alechania Misturini[a], Victoria Moreno[d], Jose Luis Jordá[a], Germán Sastre[a], Sibele Berenice Castellã Pergher[b], Pablo Botella[a,*]

[a] *Instituto de Tecnología Química, Universitat Politècnica de València-Consejo Superior de Investigaciones Científicas, Avenida de los Naranjos s/n, 46022 Valencia, Spain*

[b] *Universidade Federal do Rio Grande do Norte, Laboratório de Peneiras Moleculares, Instituto de Química, 59078-970 Natal, RN, Brazil*

[c] *Instituto de Instrumentación para Imagen Molecular (I3M), Centro Mixto CSIC-Universitat Politècnica de València, Camino de Vera s/n, 46022 Valencia, Spain*

[d] *Centro Investigación Príncipe Felipe, C/Eduardo Primo Yúfera 3, Valencia 46012, Spain*

* To whom correspondence should be addressed. *E-mail:* pbotella@itq.upv.es. *Fax: +34 96 3879444.*

Abstract

Post-synthetic modification of covalent organic frameworks (COFs) is strongly demanded in order to provide additional functionalities to their structures. However, the introduction of functional groups during the synthesis of two dimensional COFs (2D COFs) is highly discouraged, as they can interfere with the π−π stacking forces, compromising framework integrity. Here, we show that direct incorporation of nucleophyllic groups (e.g., primary amines) on pore wall during the synthesis of a 2D-COF (COF-5) is possible by sequential substitution of original monomers. Subsequent bonding of the antitumor drug camptothecin results in a stable hydrophobic drug delivery system. Water adsorption isotherms modelling indicates that the insertion of CPT ligand in the framework promotes a hydrophobic effect that protects a region of COF chain from boronate ester hydrolysis and resulting degradation, which is also proven by stability testing in physiological conditions. Furthermore, this hydrophobic nature favors cell internalization kinetics by promoting interactions with the lipophilic cell membrane. To the best of our knowledge, this is the first case of a stable drug delivery system based on covalently conjugated COFs.

***Keywords*:**

Covalent Organic Framework, Sequential Functionalization, Framework Stability, Water Adsorption Isotherms, Drug Delivery Systems, Camptothecin.

1. Introduction

Covalent organic frameworks (COFs) are a brand new target of research in porous materials, as they combine high crystallinity, defined pore size and large external surface area with a fully organic (mostly biodegradable) composition [1]. These materials show strong potential for multiple applications such as gas adsorption, catalysis, molecular separation, energy storage and proton conduction, among others [2–7]. Also, very recently, they have been proposed as potential carriers for drug delivery systems [8–11]. Particular interest is devoted to two dimensional COFs (2D-COFs), which assemble via dispersive forces (π-stacking) into highly crystalline structures [12,13]. These are built by condensation reactions, including the formation of B-O, C-N, B-N and B-O-Si bonds, to give fairly crystalline frameworks. Furthermore, the post-synthetic modification of these materials (e.g., with therapeutic molecules for drug delivery) provides additional functionalities. Unfortunately, the incorporation of functional groups during the synthesis of 2D COFs as anchoring points for subsequent covalent linking is challenging, as they can interfere with the π–π interactions, which compromises framework integrity [14,15]. Actually, a few cases have been proposed by introduction of azide [16], allyl [17] or alkyl [18] groups. Very recently, Bein and co-workers have pointed out the benefits of functionalizing COF structure with a nucleophyllic functional group such as a primary amine [19,20]. For this sake, they carried out the condensation of the pristine framework with nitro functionalities and, subsequently, these were reduced to afford an amino functionalized COF, which can be reacted with carboxyl moieties through amide bonding.

In this work, we propose for the first time the direct incorporation of primary amino groups on pore wall during the synthesis of a 2D-COF by stepwise substitution of original

monomers. We have selected COF-5 for this study because of its wide pore size [21], which makes it suitable for further linking of bulky molecules, as the antitumor drug camptothecin (CPT). In addition, we show that CPT incorporation in COF-5 provides good resistance to hydrolytic digestion, which is related to the hydrophobic profile associated to the high concentration of CPT molecules inside the pores. By modelling water adsorption isotherms, we prove that internal water diffusion is clearly constrained in the CPT functionalized structure. To the best of our knowledge, this is the first report on a stable drug delivery system (DDS) based on covalently modified COFs.

2. Experimental

2.1. Reagents and cells

Camptothecin (CPT) and 4-(tert-butoxy)-4-oxobutanoic acid (TBOA) were purchased from Fluorochem. Benzene-1,4-diboronic acid (BDBA) and 2,3,6,7,10,11-hexahydroxytriphenylene hydrate (HHTP) were obtained from ABCR. Nitric acid 90 %, urea, palladium on carbon (10 wt%), 4-(dimethylamino)pyridine (DMAP), *N,N'*-diisopropylcarbodiimide (DIC), 1-ethyl-3-(3-dimethylamino-propyl)carbodiimide hydrochloride (EDC), 1-Hydroxybenzotriazole hydrate (HOBT), *N,N*-diisopropyl-ethylamine (DIPEA) and anhydrous solvents were provided by Sigma-Aldrich. Alexa Fluor 647 (AF647) *N*-hydroxy succinimide (NHS) ester was purchased from Jena Bioscience. HPLC grade solvents were supplied by Scharlab. Water was deionized to 18.2 MΩ cm^{-1} using a milliQ pack system. Human cervix carcinoma cell line (HeLa) and human breast carcinoma cell line (MCF-7) were obtained from American Type Cell Culture (ATCC, Rockfield, MD) and cultured in Dulbecco's Modified Eagle Medium (DMEM) supplemented with 10 % fetal bovine serum (FBS, from Lonza, Verviers, Belgium) and 1 % penicillin and streptomycin (from Gibco) under a humidified atmosphere (5 % CO_2) at 37 °C. L929 mouse fibroblast cells were obtained from ATTCC

and maintained in DMEM supplemented with 10% FBS, 1% penicillin and streptomycin (P/S), 2 mM L-glutamine and 1% L-glucose, under a humidified atmosphere (5 % CO_2) at 37 °C.

2.2. Preparation of amino-functionalized COFs

2.2.1. Synthesis of 2-aminobenzene-1,4-diboronic acid (BDBN)

BDBA was modified in two steps (nitration and reduction with H_2) following a modified protocol [22]. Firstly, 30 mL of 90 % nitric acid was cooled down to 0 °C for 15 min. Afterwards, 100 mg of urea was added and the mixture was cooled down to -10 °C. Then, 5 g of BDBA (30.2 mmol) was added in small portions under strong stirring for 1 h. After complete addition of BDBA, magnetic stirring of the resulting mixture was continued at -10 °C for 15 min. Then, the red-dark solution was poured into a beaker on ice with a small amount of water. After filtration, the precipitate was washed with water and dried under vacuum, recovering 3.817 g (60% yield) of 2-nitrobenzene-1,4-diboronic acid (NO_2-BDBA) as a light yellow solid. In a second step, a solution of 0.5 g of NO_2-BDBA in a mixture of 10 mL methanol and 0.2 mL of HCl 36.5% containing 0.150 g of palladium on carbon (Pd/C, 10% wt Pd) was hydrogenated at room temperature (H_2 10 bar) for 1 hour under stirring. The Pd/C catalyst was separated by filtration with Celite® and the solvent was removed under reduced pressure to obtain 0.497 g (99.4 % yield) of BDBN as a white solid. Characterization data of intermediate and final products are shown at the Supplementary Information.

2.2.2. Synthesis of COF-5 and CF-x (x=25-100)

COF-5 and derivatives were prepared by optimizing a known recipe [21]. For the synthesis of CF-*x* samples, BDBA was sequentially substituted by BDBN (**1b**) (where *x* is BDBN fraction in total bencene-1,4-diboronic ligand). Initially, 187 mg (1.13 mmol)

of BDBA and 243 mg (0.75 mmol) of HHTP were introduced into a Schlenk tube. The mixture was purged with N_2 (three N_2/vacuum cycles) to remove any trace of humidity. Then, 20 mL of a mixture of 1,4-dioxane:mesitylene (1:1 v/v) were added. The resulting suspension was sonicated for 10 min, ultra-rapid frozen with liquid nitrogen and purged again with N_2 as described above. The reaction mixture was heated at 100 °C during 3 days. Afterwards, the gray-purple solid was recovered by filtration, washed with anhydrous toluene and dried overnight at room temperature under vacuum to give 295 mg of COF-5 (CF-0, 80.4 % yield). Subsequently, sequential incorporation of BDBN to replace BDBA was performed to give CF-*x* materials.

2.3. Preparation of CPT-functionalized ligands and materials

2.3.1. Synthesis of camptothecin-20-O-hemisuccinate (CPT-Suc)

CPT prodrug was synthesized by fitting a previously reported method [23]. 1.002 g (5.75 mmol) of 4-(tert-butoxy)-4-oxobutanoic acid (*t*-Suc) and 0.473 g (3.89 mmol) of DMAP were dissolved in 200 mL of anhydrous dichloromethane (DCM). Then, 1.1 mL (7.10 mmol) of DIC and 1.022 g (2.93 mmol) of CPT were added and left with constant stirring overnight. Afterwards, the mixture was washed with 0.1 M HCl, dried over anhydrous Na_2SO_4, filtered and evaporated to dryness. The solid was purified by recrystallization from methanol. After drying, the solid was dissolved in 30 mL of DCM and treated with 20 mL of trifluoroacetic acid (TFA) for 1 h at room temperature with magnetic stirring, and then the product was evaporated to dryness. The residue obtained was purified by recrystallization from methanol at 4 °C for 3 days. Finally, the solid obtained (CPT-Suc) was filtered and washed with cold methanol and dried under vacuum. The yield of synthesis was 90.4% (1.184 g, 2.65 mmol). Characterization data of final product are shown at the Supplementary Information.

2.3.2. Incorporation of camptothecin to amino functionalized COFs

0.200 g of CF-25 was dried at 100 °C under vacuum for 24 h. In parallel, 0.166 g (0.372 mmol) of CPT-Suc, HATU (170 mg, 0.446 mmol) and N,N'-diidopropylethylamine (DIPEA, 156 µL, 0.892 mmol) were added to the mixture. Then, the reaction was stirred at room temperature during 2 days under argon atmosphere. Finally, the resulting grey solid was filtered and washed with anhydrous DCM to obtain 221 mg of CF-25-CPT.

For the sake of comparison, CF-25 with adsorbed CPT (CF-25/CPT) was prepared *via* diffusion of the drug through the pores. Briefly, 150 mg of drug was dissolved in 50 mL of anhydrous DCM. Then, 150 mg of CF-25 was added and the mixture was stirred for 12 h at room temperature. After this time, the mixture was filtered, washed with anhydrous DCM and dried under vacuum to give 155 mg of dark grey solid.

2.3.3. Incorporation of Alexa Fluor 647 (AF647) to amino functionalized COFs

CF-25 and CF-25-CPT were labeled with AF647 for flow cytometry assays *via* covalent conjugation between NHS-ester group of fluorescent probe and material amino groups, using a procedure described in the literature [24]. For this purpose, 10 mg of previously dried under vacuum CF-25-CPT were suspended in 9.75 mL of anhydrous DCM. Then, 250 µL of AF647 solution (1 mg/mL in anhydrous dimethyl sulfoxide, DMSO) were added and the mixture was stirred at room temperature in dark for 2 hours. Afterwards, supernatants were separated by centrifugation (16100 G) at 4 °C, washed with anhydrous DCM (3 x 10 mL) and dried under vacuum.

2.3.4. Camptothecin quantification

CPT total amount was determined by complete hydrolysis in alkaline medium. In this way, amide bonds between CPT molecules and COF-NH_2 are hydrolyzed, and the CPT carboxylate form is released. For this purpose, 1 mg of the conjugate (CF-25-CPT or CF-25/CPT) was suspended in

1 mL of NaOH 0.03 M at 37 °C in a Thermomixer (1500 rpm). After 3 h, the supernatant was separated by centrifugation (16100 G) at 4 °C, dried under vacuum and reconstituted with MeOH-HCl (95:5 v/v). Finally, CPT was quantified by reverse-phase high performance liquid chromatography (RP-HPLC) analysis on an Agilent HPLC 1220 Infinity LC coupled to a fluorescence detector 1260 Infinity with a C-18 reverse phase column (MEDITERRANEA SEA18, 5 μm, 25 × 0.46 mm, Teknokroma, Sant Cugat del Vallés, Spain). The products were eluted utilizing a constant solvent mixture (CH_3CN/H_2O-TFA pH 4.5 50:50 v/v) at 0.8 mL min^{-1}. 20 μL of standards and resulting solutions were injected. All determinations were done in triplicate.

2.4. Stability in aqueous medium

To investigate the hydrolytic stability of CPT loaded materials we carried out three different studies.

2.4.1. Water adsorption isotherms and mechanical properties calculation

COF-5 (CF-0), CF-25 and CF-25-CPT structural models were considered. The framework structure of CF-0 was obtained from available crystallographic data [25]. This was modified by the insertion of the ligand and amino groups at all benzene linkers to obtain CF/25 and CF-25-CPT framework. All structures were optimized at constant pressure using Universal Force Field (UFF) [26] at GULP package (version 4.3.2) [27], followed by Young modulus calculation, in order to evaluate the stiffness of studied COFs, measuring framework deformation when a force is applied. This value is obtained by the ratio of stress to strain at each axis.

Water adsorption isotherms over CF-0, CF-25 and CF-25-CPT were determined through Gran Canonical Monte Carlo (GCMC) simulations, performed with RASPA software package (version 2.0.35) [28]. GCMC simulations have been carried out at 300 K and at pressures ranging from 1.0×10^{-5} to 10.0 bar, for 10^4 initiation cycles and 5×10^5

production cycles. Water molecules were described by the SPC/E model [29], which reproduces bulk properties of liquid water when compared with other rigid three point charge models available [30]. COFs frameworks were kept fixed during simulation and its interaction with water was modeled by means of Coulombic and Van der Waals contributions. For the first, the atomic charges at PBE0/Def2-TZVP [31] level of theory were calculated with software Gaussian (v 09) [32], and for the latter, Lennard-Jones parameters were obtained from an expansion of CHARMM force field for boron-containing compounds [33]. Other missing parameters were obtained from an expansion of AMBER force field for aryl boronic acids [34].

2.4.2. Framework stability

^{1}H-NMR was used to monitor the release of BDBA monomer over time under water exposure [35]. 1 mg of dry and finely ground CF-25-CPT or CF-25 material was placed in a NMR tube and 0.7 mL of D_2O was added. Benzene was used as internal standard (1 mL). NMR scans were run at specific times, extending up to 24 h.

2.4.3. Camptothecin release

CPT release from drug-loaded samples was determined in phosphate buffer saline solution (PBS, 1x, pH 7.4). Briefly, 1 mg of CF-25-CPT or CF-25/CPT was dispersed in 1 mL of PBS in an Eppendorf tube and shaken in a Thermomixer® at 1500 rpm and 37 °C. At the corresponding time points, samples were centrifuged (16200 G, 15 min) and the supernatant was freeze-dried. Alternatively, the release test was carried out in DMEM medium supplemented with 10% FBS and 1% antibiotic (streptomycin/penicillin). In this case, samples were centrifuged (21,100 G, 15 min), and the supernatant was treated with 500 mL of 5% aqueous solution of trichloroacetic acid at 4 °C to precipitate serum proteins, which were separated after centrifugation (6200 G, 10 min) prior to freeze-

drying. Finally, all samples were reconstituted with 2 mL of MeOH-HCl 95:5 (v/v) and CPT and derivatives were validated by RP-HPLC as described. When needed, Quadrupole time-of-flight mass spectra (Q-TOF/MS) were recorded on an Aquity UPLC Waters coupled with Xevo Q-TOF MS with an Aquity UPLC BEH C18 (1.7µm, 50 x 21 mm) column and using positive electrospray ionization. The products were eluted utilizing a constant solvent mixture 50:50 v/v (solvent A = 0.1 % CH_3COOH/CH_3CN; solvent B = H_2O) at 0.5 mL min^{-1}. All determinations were carried out in triplicate.

2.5. Materials characterization

XRD patterns were collected in a Philips X'Pert diffractometer equipped with a graphite monochromator, operating at 40 kV and 45 mA and using nickel-filtered Cu Kα radiation (λ = 0.1542 nm). Liquid nitrogen adsorption-desorption isotherms were measured at 77 K in a Micromeritics Flowsorb apparatus. Surface area calculations were done by the BET method. In addition, pore diameter distributions were calculated from argon adsorption-desorption isotherms measured at 4 K after using the Horvath-Kawazoe model. Fourier transform infrared spectra (FTIR) were recorded at room temperature in the 400-3900 cm^{-1} region with a Nicolet 205xB spectrophotometer, equipped with a Data Station, at a spectral resolution of 1 cm^{-1} and accumulations of 128 scans. Absorption spectra were recorded in a Cary 50 spectrophotometer (Varian) by using quartz cuvettes with 10 mm optical path lengths. Fluorescence experiments were carried out in a Photon Technology International (PTI) LPS-220B spectrofluorometer at an excitation wavelength λ_{exc}=350 nm. All measurements were performed in a quartz cuvette with 10 mm optical path lengths. Magic angle Spinning-Nuclear magnetic resonance (MAS-NMR) spectra were obtained at room temperature on a Bruker AV400 spectrometer, with a 7 mm Bruker BL-7 probe at sample spinning rate of 5 kHz. The ^{1}H to ^{13}C cross-polarization spectra were acquired by using a 90 pulse for ^{1}H of 5 µs, a contact time of 5

ms and a recycle of 3 s, and referred to adamantine. Samples for transmission electron microscopy (TEM) were ultrasonically dispersed in 2-propanol and transferred to carbon coated copper grids. TEM micrographs were collected in a JEOL JEM 2100F microscope operating at 200 kV. Particle average diameter was calculated as the media with standard deviation of at least 250 measured nanoparticles. Elemental analysis were carried out in a FISONS, EA 1108 CHNS-O equipment.

2.6. Biological validation

2.6.1. Cell internalization assays

Quantitative cell internalization determinations were carried out firstly by flow cytometry (FC). For this purpose, HeLa cells were seeded in 12-well plates at a density of 80,000 cells/well and allowed to attach for 24 h. Then, AF647-labeled nanomaterial (CF-25-CPT) was added to wells (in triplicate) at a final concentration of 1 and 5 μg mL^{-1} and maintained for 6 additional hours. After repetitively washing with PBS, adhered cells were trypsinized, carefully collected in DMEM and treated with 2 μL of DRAQ 5™. Flow cytometric analyses were performed in a FC500 MPL Flow Cytometer (Beckman-Coulter). Data were analyzed and plotted for AF647 and DRAQ 5^{TM} in a two-way dot plot. Previously, calibration was carried out for two different gated regions: cells stained with DRAQ 5^{TM} and no nanoparticles, and cells stained with DRAQ 5^{TM} and AF647-labelled nanoparticles. All data were expressed as mean ± standard deviation (SD).

Additional cell uptake studies of nanoparticles in HeLa cells were monitored by laser confocal scanning microscopy (LCSM). For this purpose, 150000 cells/well were seeded in 6-well plates and stabilized for 24 h at 37 °C in 95% air and 5% CO_2 environment to allow cells to attach. Then, the growth medium was exchanged and cells with fresh medium were incubated overnight with AF647-labeled CF-25, with final dose of 10 μg

mL-1. Afterwards, Lysotracker Green was introduced at a concentration of 10 μM and subsequently the supernatant was replaced with fresh medium. The nuclei were counterstained with Hoechst 33342 (final concentration of 1 μg mL^{-1}) for 15 min. Finally, the samples were visualized on a Leica TCS-SP2-AOBS confocal microscope (Leica Micro-systems CMS GmbH, Germany).

2.6.2. Cytotoxicity test

The effect of different materials on cell metabolic activity was determined using the MTT (3-[4,5-dimethylthiazol-2-yl]-2,5-diphenyl tetrazolium bromide) colorimetric assay. Cells were seeded in a 96-well plate at a density of 4000 (HeLa), 8000 (MCF-7) or 6000 (L929) cells per well and cultured in 5% CO_2 at 37 °C for 24 h. Then, cells were treated with naked materials, CPT loaded COFs or free CPT (stock solution in DMSO), with final doses ranging from 0.3 to 0.00015 μg/mL (in CPT equivalents) during 72 h. At the end of the incubation period, 10 μL of MTT solution (5 mg mL^{-1}) in culture medium was added into each well and incubated for another 4 h. The supernatant in each well was carefully removed and 150 μL of isopropanol was added to dissolve formazan crystals. Absorbance was measured with a Perkin Elmer Wallac 1420 VICTOR2 Multilabel HTS Counter (Northwolk, CT, US) at the wavelength of 570 nm. IC_{50} survival data were calculated by nonlinear regression sigmoidal dose-response (variable slope) curve-fitting using Prism 6.0 software (GraphPad, San Diego, CA). Three independent experiments were performed for every sample and each experiment was carried out by in triplicate.

3. Results and discussion

3.1. Amino-functionalized COFs

COF-5 (denoted as CF-0) was obtained by an optimized synthesis method through condensation of BDBA and HHTP in a 1:1 (v/v) solvent mixture of 1,4-dioxane and

mesitylene [20]. In parallel, BDBN was prepared by BDBA nitration and further reduction of the nitro group. Then, BDBA was sequentially substituted in the synthesis by BDBN to give CF-*x*, *x*=25-100 (Fig. 1), where *x* corresponds to the BDBN fraction expressed as % (Table 1).

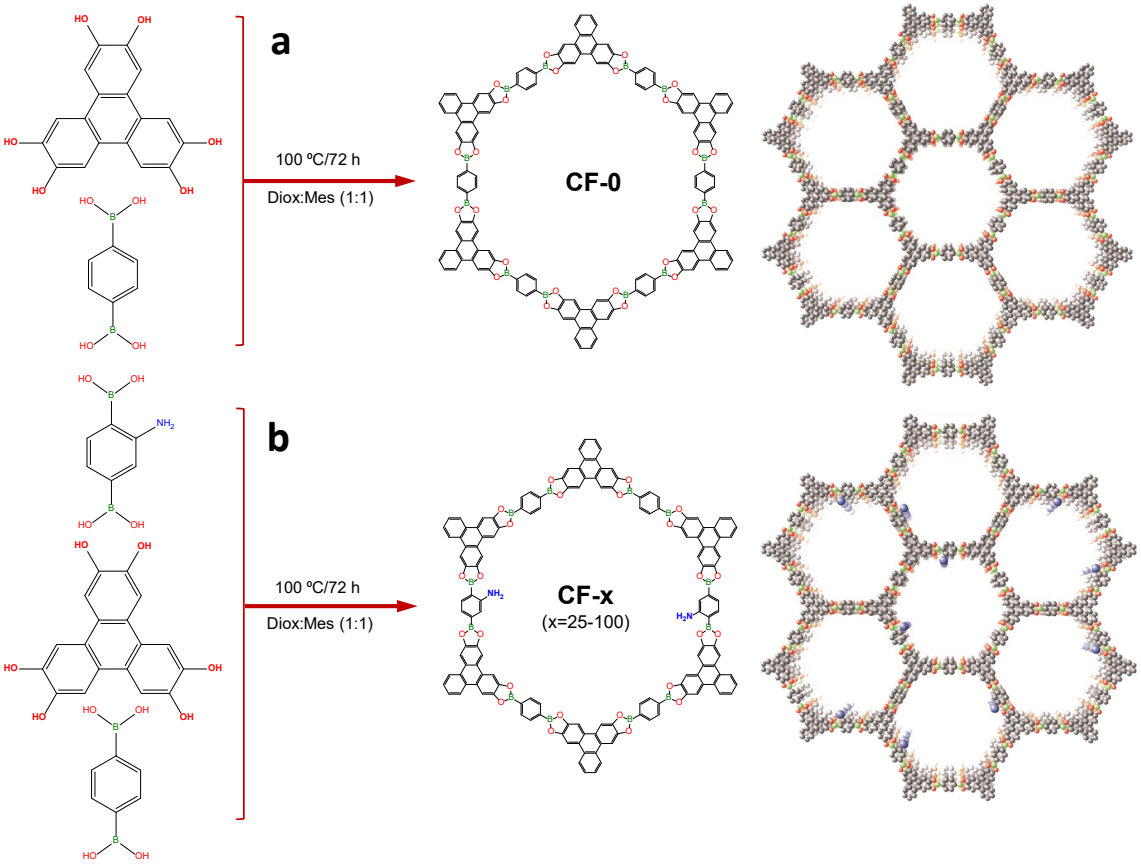

Fig. 1. (a) Synthesis scheme of COF-5 via condensation of benzene-1,4-diboronic acid (BDBA) and 2,3,6,7,10,11-hexahydroxytri-phenylene (HHTP) in a mixture of 1,4-dioxane (Diox):mesitylene (Mes) (1:1 v/v). (b) Synthesis scheme of CF-*x* series through stepwise substitution of BDBA by 2-aminobenzene-1,4-diboronic acid (BDBN).

The effect of BDBA substitution over COF-5 crystallinity was monitored by powder X-ray diffraction (Fig. 2a). We were successful to incorporate primary amino groups to COF-5 framework by this method up to *x*=60. Beyond this limit, the structure becomes unstable and mayor reflections correspond to unreacted species (Fig. S1 in the Supplementary Data). This result is similar to that pointed out by Bein and co-workers

for the introduction of thiol and carboxylate groups in COF-5 framework [20]. Indeed, the incorporation of BDBN in COF-5 framework led first to enhance of crystallinity, which was apparent according to a sharpening of the main XRD reflections. In order to quantify this effect, we estimated the extension of crystalline domains in the different materials by application over the (*100*) reflection of the Scherrer formula (see Supplementary Data). The obtained results were compiled in Fig. S2 in the Supplementary Data, which shows that the presence of the amino ligand in CF-25 structure provokes a modest enlargement of crystalline domains. Conversely, additional BDBN substitution ($x \geq 40$) led to quick reduction of crystalline domains, probably due to the strong interference that amino groups in high concentration may deploy over the π–π interlayer interactions in 2D structure. A small HHTP impurity was also present for amino functionalized materials. We could not remove it even after a thoroughly activation step with acetone [18,19,21], probably due to its large molecular dimensions and strong electronic interactions with amino groups within COF-5 channels. Moreover, little improvement was achieved by washing out the sample in a reflux of acetone, and the crystallinity decreased dramatically. Other solvents with high cleaning strength, as DMSO or MEK, destroyed completely COF structure. In any case, this small impurity did not affect to crystallinity, and XRD patterns were indexed unambiguously to a *P6/mmm* symmetry. Here, Rietveld refinement produced lattice parameters of $a=b=29.5$ Å and $c=3.4$ Å for $x=25$, $a=b=29.4$ Å and $c=3.4$ Å for $x=40$ and $a=b=29.5$ Å and $c=3.4$ Å for $x=60$.

Surface area and pore volume were calculated from N_2 adsorption-desorption isotherms (Fig. 2b-d and Table S1 in the Supplementary Information). Unmodified COF-5 material presented a surface area of 1622 $m^2\ g^{-1}$ and a pore volume of 0.82 $cm^3\ g^{-1}$, which are in line with those reported in the original synthesis [21]. Then, the partial substitution of

BDBA by BDBN (x=25) produced initially a small increase (over 10%) of surface area (1791 m^2 g^{-1}) with no changes in pore volume. As commented before, this is consistent with the development of a highly crystalline network with fully open and accessible pores in the amino functionalized material. Actually, the profile of observed sorption isotherms stresses the very-well developed porosity of this structure. A similar case was reported by Bein and co-workers by introducing a monoboronic acid as modulator in the synthesis of COF-5 [20]. However, a further increase of BDBN substitution (x≥40) led to dramatic porosity reduction, which is attributed to the reduction of crystalline domains and severe pore blocking caused by HHTP retained molecules. Moreover, for x>60 the structure collapsed, with very low surface area and pore volume. Pore size analysis (as determined by Horvath-Kawazoe model) indicated that BDBN incorporation in COF-5 framework does not modify pore size (estimated over 2.6 nm), but it defines less uniform pores and increases the contribution of textural porosity. These results match reasonably well those obtained via non local density functional theory (NLDFT) by other authors [16,20,21].

Table 1

Initial composition used for the synthesis of COF-5 and CF-x amine derivatives.

Samples (CF-x)	x [%]	Molar Ratio (BDBA:HHTP:BDBN)	Synthesis Composition						Yield (%)
			HHTP (mg)	HHTP (mmol)	BDBA (mg)	BDBA (mmol)	BDBN (mg)	BDBN (mmol)	
CF-0	0	3.00 : 2 : 0.00	243	0.75	187	1.13	---	---	80.6
CF-25	25	2.26 : 2 : 0.77	243	0.75	156	0.85	51	0.28	78.4
CF-40	40	1.80 : 2 : 1.22	243	0.75	140	0.68	82	0.46	82.2
CF-60	57	1.22 : 2 : 1.81	243	0.75	113	0.45	122	0.68	92.3
CF-70	71	0.90 : 2 : 2.11	243	0.75	93	0.34	143	0.79	80.4
CF-80	78	0.60 : 2 : 2.41	243	0.75	76	0.23	163	0.90	74.1
CF-100	100	0.00 : 2 : 3.00	243	0.75	---	0.00	204	1.13	82.5

Infrared spectra (FTIR) of COF-5 and CF-x series are shown in Fig. 2e. CF-0 presents the expected boronate ester ring stretching signals at 1348 cm^{-1} and 1328 cm^{-1}. However, in the amino functionalized materials the band at 1348 cm^{-1} is

clearly shifted to higher energy, whereas the shoulder at 1328 cm^{-1} disappears. This is due to the intramolecular interaction between B-O and NH_2 moieties [36,37].

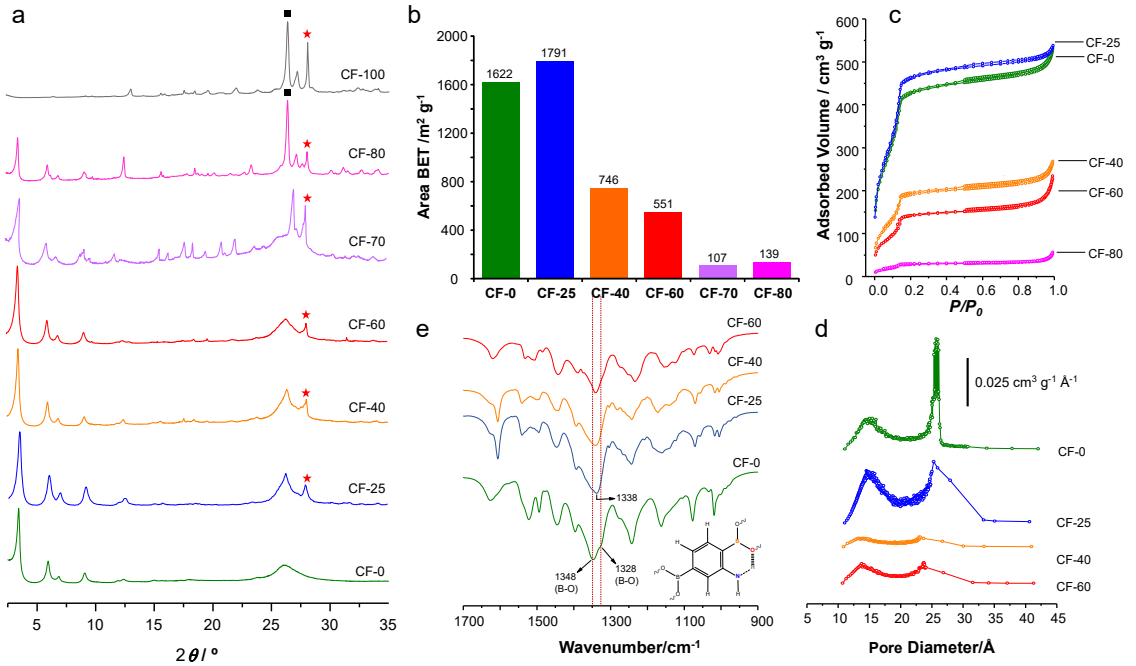

Fig. 2. (a) Powder XRD patterns of CF-*x* series. Legend: (★) HHTP, (■) BDBN. (b) BET surface areas of CF-*x* materials as calculated from the nitrogen adsorption-desorption isotherms. (c) Nitrogen adsorption-desorption isotherms of as-prepared CF-*x* series acquired at 77 K. (d) Pore size distribution calculated for CF-*x* series from argon adsorption-desorption isotherms acquired at 4 K by using a Horvarth-Kawazoe slit pore geometry model. No readable report was obtained for *x*>60. (e) FTIR spectra of CF-*x* series showing the shifting of boronate ester ring stretching signals to higher energy due to the intramolecular interaction between B-O and NH_2 moieties.

Electronic microscopy (TEM) images for CF-0 sample displayed typical hexagonal arrangement and large intergrowth domains (e.g., 20-30 nm, Fig. 3a). However, the incorporation of primary amino groups produced small nanoparticles of about 85.0±20.8 nm avg. diameter for *x*=25 (Fig. 3b).

Post-synthetic functionalization of CF-*x* materials requires to precisely determine the real level of substitution in every case. This was done through a quantitative compositional analysis of CF-*x* samples by ^{1}H-NMR. Samples were dissolved in deuterated dimethyl sulfoxide (DMSO-d_6) with pinacol. Proton NMR signals of

HTTP and the pinacol conjugates of BDBA and BDBN were integrated and normalized (Fig. S3 and Table S2 in the Supplementary Data). The unmodified COF-5 showed a HHTP:BDBA ratio of 1:1.06, which is consistent with other authors' results.[16] For *x*=25-60, the obtained percentage of substitution was very similar to the initial molar composition (*x*=25, 18% final substitution; *x*=40, 41%; *x*=60, 60%), providing lots of anchoring points for covalent linking of functional molecules.

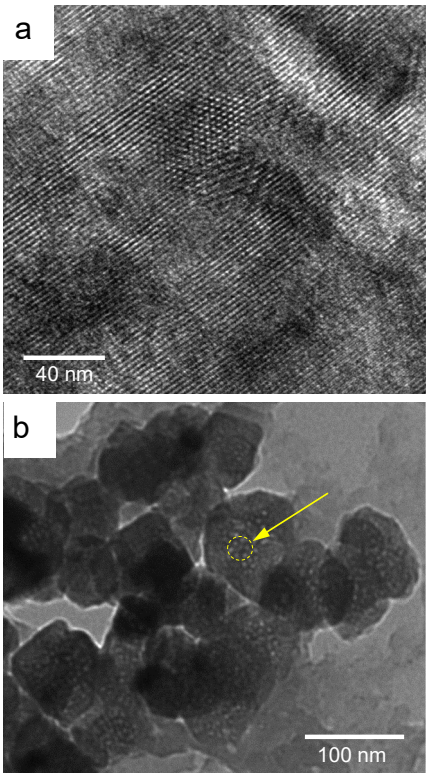

Fig. 3. TEM micrographs. (a) Unambiguous *P6/mmm* symmetry and large intergrowth domains of pristine COF-5 are clearly seen at (b). Nanoparticles of CF-25 material showing the hexagonal symmetry (arrow).

3.2. CPT-functionalized COFs

Therefore, we have successfully achieved NH_2-pore functionalization of COF-5 in a one-pot protocol. To check the accessibility of primary amino groups to post-synthetic modification we tried the incorporation of a therapeutic molecule, in order to give a novel DDS. Despite their high surface area and internal ordered porosity, COF application as

DDSs is currently limited by two severe drawbacks: i) structure stability in aqueous medium, and ii) unspecific drug release of therapeutic load before reaching the target cells, as drug molecules are incorporated by a simple adsorption strategy. Only a few cases have been reported of COFs as DDSs [38–41]. For this study we chose CF-25 sample due to its superior BET surface area. We performed an amidation reaction between amino groups of CF-25 and camptothecin-20-*O*-hemissucinate, to give the corresponding camptothecin (CPT) derivative material (CF-25-CPT, Fig. S4). Electronic microscopy (TEM) showed no significant structural changes in COF-5 framework with regards CF-25 pristine material (Fig. S5). Furthermore, particle size was not significantly affected by CPT incorporation (88.0 ± 25.7 nm, avg. diameter).

XRD report (Fig. S6a) confirmed no change in crystallinity in the drug-containing sample, and the observed pattern corresponded to the initial AA stacking (*P6/mmm*) of COF-5 [42]. At this point, it has been reported that the incorporation of bulky substituents inside COF channels can exert significant influence on the topology of COFs, mostly modifying the π–π stacking model from the stable eclipsed packing (AA) to other layer arrangement (staggered AB or ABC, inclined or serrated) [42–44]. However, in our case no deviations from the ideal model were detected, at least at the range of CPT loading achieved. Actually, as commented before, CF-25 presents only 18% BDBN in the framework, corresponding to a 2.60% (wt/wt) nitrogen content (as determined by Elemental Analysis). Then, CF-25-CPT has 3% CPT (wt/wt), which represents an occupation of about 5% amino groups. This result is in line with those reported by Cui and co-workers [44], who described that the incorporation of suitable substituents into the skeleton of 2D COFs could lead to steric repulsion between layer substituents, affecting to the stability of the COF structure. Specifically, they introduced ethyl and isopropyl ligands in variable quantity, observing a progressive modification of the initial

AA stacking to other conformations (AB or ABC). However, for substitution level lower than 10% there was no significant changes in the stacking mode.

Moreover, Rietveld refinement of the experimental data according to the *P6/mmm* symmetric model gave almost identical lattice parameters than CF-25: a=b=29.9 Å and c=3.4 Å .

Conversely, the introduction of the CPT-Suc moiety inside the channels led to a dramatic reduction of porosity (Fig. S6b), due to severe pore blocking (BET surface area = 482.9 $m^2\ g^{-1}$; pore volume = 0.01 $cm^3\ g^{-1}$).

The successful incorporation of the drug was confirmed via UV−Vis diffuse reflectance measurements (Figure S6c). While the CF-25 absorbs strongly at wavelengths below 350 nm, its absorption above this range is very low and free of spectral features. The attachment of CPT gave rise to a sharp absorption peak at 374 nm [45]. Moreover, fluorescence measurements also helped to assess the presence of CPT in CF-25 framework (Figure S6d). Upon excitation at 350 nm the CPT modified material exhibits a broad emission centered at 420 nm [46]. Here, it must be stressed that both the absorption and emission spectra are red-shifted and broadened with regards the spectra of the drug in solution, as expected when the molecule is immobilized at a surface [20]. Covalent linking of CPT to CF-25 was also confirmed by ^{13}C-MAS-NMR (Fig. S6e). The peak at 160 ppm corresponds to the C=O group of the amide moiety.

CPT loading was monitored by complete hydrolysis in alkaline medium and further quantification by RP-HPLC, and the CF-25 material showed significant capability to incorporate the active molecule over pore walls (3% CPT wt/wt). As this drug loading level was enough for therapeutic studies we didn’t try any further addition, in order to preserve COF textural properties.

3.3. Stability in aqueous medium

As commented, the stability in physiological conditions is a key parameter for DDSs. In this context, COF-5 shows typical high susceptibility to humidity of boronate ester-linked polymers, which in this case is emphasized by material large pore [37]. Therefore, to validate the stability of CF-25-CPT sample in aqueous medium we first determined water adsorption isotherms in a wide range of pressure. Then, we monitored resistance to hydrolysis by ^{1}H-NMR and, finally, CPT release in PBS was quantified by RP-HPLC.

Optimized structures of CF-0, CF-25 and CF-25-CPT and atomic charges calculated are summarized at Fig. S7-S10. While the pristine COF kept its structure almost unchanged from crystallographic data, when incorporating CPT ligand the optimized structure adopts a conformation that maximizes its interaction with the side of CF-25-CPT sheets (Fig. 4). As the ligand stretches towards the cavity, the final conformation allows dispersive interactions between the COF and ligand aromatic moieties, as well as hydrogen bonds with 5 of the 8 sheets in CF-25-CPT model.

Water adsorption isotherms were calculated over CF-0, CF-25 and CF-25-CPT (Fig. 5a) by using structural models containing 8 layers with their previously optimized structures. Final conformations from GCMC simulations at 0.01 bar of investigated materials are illustrated at Fig. 5b-d. Compared to CF-0, the addition of amino groups (CF-25) increases the water adsorption for pressures higher than 0.01 bar, as the greater polarity of substituents enhances its interactions with water molecules. Conversely, the covalent bonding of CPT-Suc to COF framework decreases the water adsorbed by CF-25 about 15%, highlighting the hydrophobic effect promoted by the ligand incorporation. The maximum loading of water

calculated follows the trend CF-25 (69.0 mmol g^{-1}) > CF-0 (67.0 mmol g^{-1}) > CF-25-CPT (58.7 mmol g^{-1}), and are almost the same for the 3 higher values of pressure computed, indicating the cavities were saturated of water. In this sense, CPT is a bulky and hydrophobic ligand that limits internal water diffusion, and protects hydrolytically susceptible boronate backbone from an immediate collapse in aqueous medium, giving longer stability to the substituted material. The uniform solvation of CF-0 and CF-25 framework (Fig. 5b-c) is affected at the ligand region on CF-25-CPT (Fig. 5d), illustrating the hydrophobic effect responsible for the decrease of water adsorption.

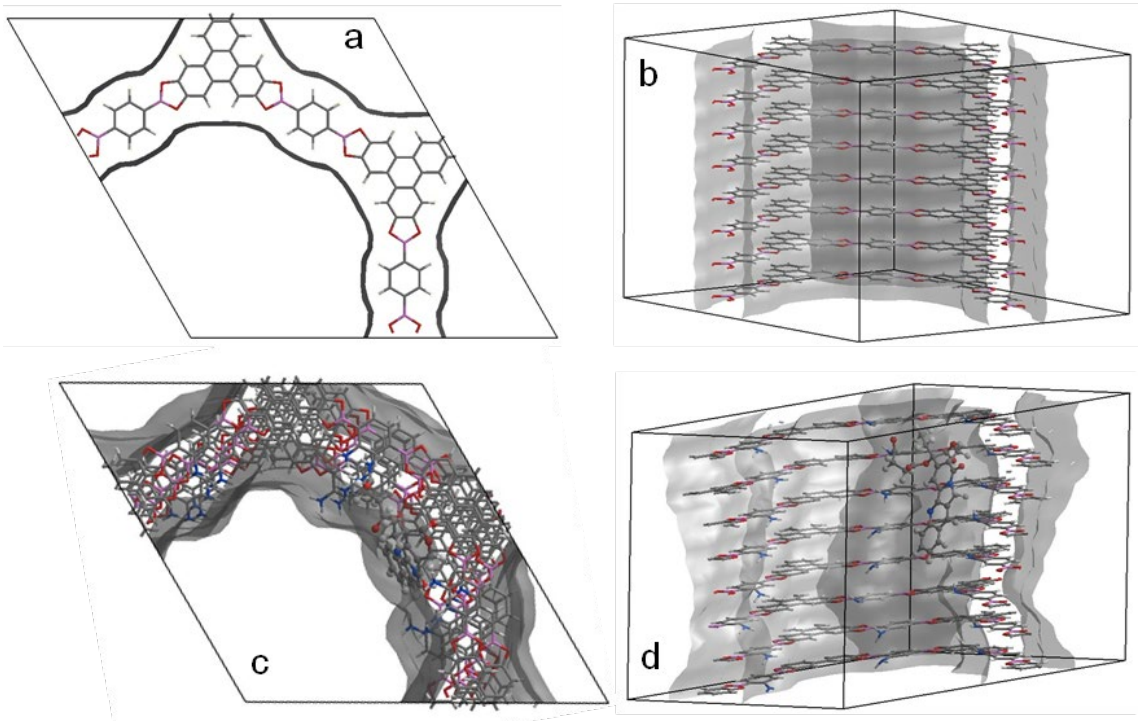

Fig. 4. Top and side view of CF-0 -b) and CF-25-CPT (c-d) optimized structures, respectively, used on water adsorption isotherms calculations.

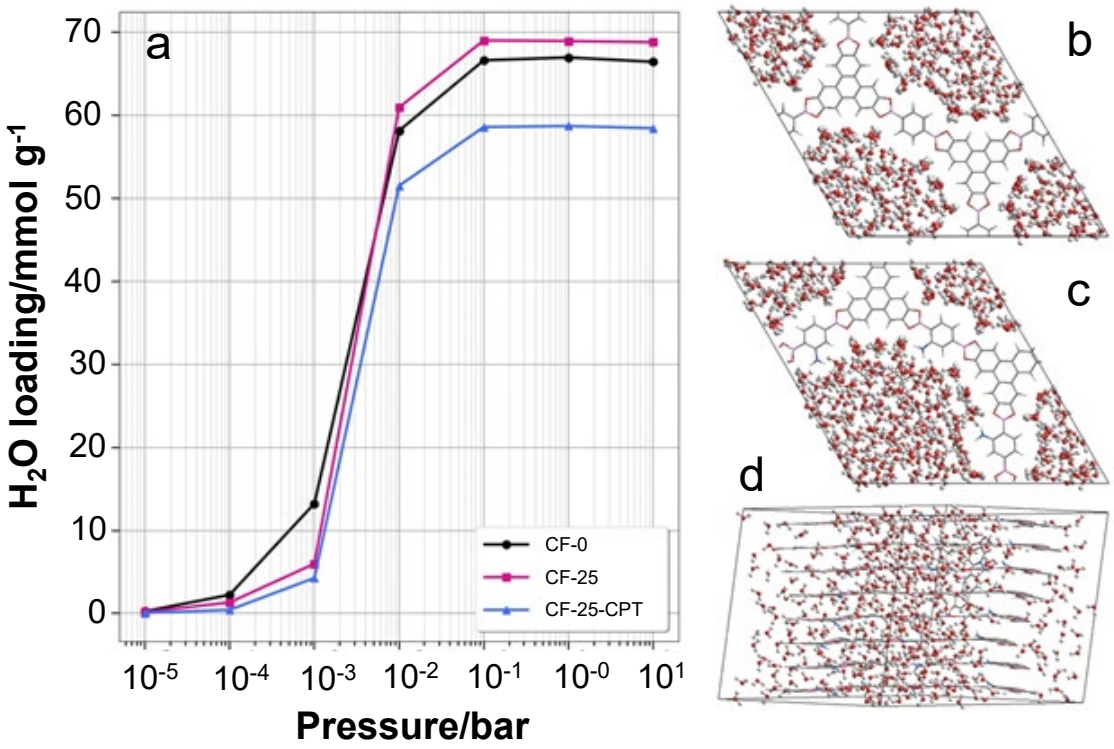

Fig. 5. Water adsorption simulation on CF-0, CF-25 and CF-25-CPT materials (a), and final configurations from GCMC simulations of CF-0 (b), CF-25 (c) and CF-25-CPT at 0.01 bar.

In addition, all geometries from GCMC simulations corresponding to adsorbed water at variable pressure are presented at Fig. S11-S13 in the Supplementary Data. The effect of covalent incorporation of hydrophobic groups inside COF pores on protection against hydrolysis has already been verified by other authors, e.g., showing that longer alkyl chains may inhibit monomer release under hydrolytic conditions [35], but to our knowledge this is the first time it is shown over the internal adsorption of water molecules in COF channels and cavities.

Furthermore, in order to evaluate the possible influence of CPT-Suc ligand insertion on COF structure we calculated Young Modulus (*E*) for CF-0 and CF-25-CPT (Supplementary Data, Table S3 and Fig. S14). However, the structural modifications promoted by the ligand insertion had little influence in the *E* value, increasing 1.24 GPa the pressure supported at x axis, in which direction the ligand become close and

interacting with 5 sheets of CF-25-CPT (Figure 2a). Moreover, ligand closeness to COF framework may promote a shift among the sheets, weakening π-π stacking interactions in CF-25-CPT structure when compared with the perfectly superimposed sheets of CF-0, which results in a slight decrease of *E* at y and z axis (0.89 and 1.32 GPa, respectively). Therefore, calculations indicate that CF-25-CPT superior stability towards water does not depend on the structural stiffness increase related to ligand insertion. Conversely, water adsorption isotherms suggest that the introduction of the ligand in CF-0 promotes a hydrophobic effect that can protect a region of COF chain from boronate ester hydrolysis and subsequent degradation.

In this context, ^{1}H-NMR allowed to oversee BDBA release in D_2O from CF-0 and CF-25-CPT, by using benzene as internal standard (Fig. S15). Under framework hydrolysis BDBA shows a sharp peak at 7.72 ppm. It must be taken into account that obtained reports may not be quantitative, as the solubility of BDBA monomer in D_2O is low, and the solutions can become saturated. However, this protocol is valid to compare the different behavior under hydrolytic conditions of the unmodified COF and the CPT-loaded material. Here, BDBA signal was clear for CF-0 from the initial stage (which corresponds, approximately, to a 3-4 min exposure to D_2O, due to the delay between NMR sample preparation and measurement), and changed very little in the rest of the process. On the contrary, BDBA signal was very small for CF-25-CPT (3% CPT wt/wt) at the beginning of the experiment (0-30 min), and even after 24 h the solution was not saturated, which confirms that CPT covalent linking inside COF-5 pores improves significantly boronate framework resistance to hydrolysis. This, however, depends on the extension of material functionalization, as an additional sample containing 1.1% CPT (wt/wt) showed very limited stability in D_2O (data not shown), with an

important fraction of BDBA leached in the first hour, which confirms that protection against hydrolytic digestion is related with CPT content and water restricted diffusion inside COF-5 framework.

This is particularly relevant for biological applications as CF-25-CPT may suffer of non-specific release in physiological conditions, by direct hydrolysis of the ester bond between drug and vehicle, then discharging free CPT, or by material structure disintegration. As commented above, the continuous exposure of CF-25-CPT to the aqueous medium provokes slow hydrolysis of the boronate ester linked polymer, releasing the building ligands BDBA and BDBN. At this point, it has been described the possibility of arylboronic compounds to act as Lewis acids and catalyze the hydrolysis of amides at room temperature, where *ortho*-substituted arylboronic acids are especially active [47]. According to the mechanism of this reaction [48], it is assumed that the reaction proceeds through a hydrogen-bonded acylboronate intermediate. As a consequence, CPT-Suc is disburdened. In this context, the stability of CF-25-CPT nanoparticles was tested by incubating 1 mg/mL in PBS at 37 °C, and monitoring the released product concentration by RP-HPLC and Q-TOF/MS (Fig. 6).

CF-25-CPT discharged less than 3% total CPT in the first hour, corresponding mostly to the prodrug CPT-Suc. This release pattern is typical of residual physical adsorption, due to the large surface area and highly ordered porosity of the support. Also, a very low quantity of free CPT was also detected, probably caused by prodrug hydrolysis. Afterwards, the system kept quite stable up to 6 h, and then it began to unload increasing amounts of CPT-Suc and CPT due to structure collapse (15% total CPT in 24 h), completing the disburden process in less than 72 h. We are aware that other nanoplatforms tested for CPT intracellular delivery have

shown improved stability (see [49] and references therein). For instance, silica nanoparticles with a similar CPT content discharge only 9% of the drug after 24 h incubation in human serum [50]. In addition, nanoparticles of the amino modified MIL-101 material, disburdened 8-12% total CPT in DMEM in 48 h [51], and conjugates of β-cyclodextrine polymers and CPT released about 25% of their total loading after 24 h at physiological pH [52]. However, our objective was to evaluate material resistance to physiological conditions for an incubation time that allows to carry out *in vitro* and *in vivo* testing with no significant drug leaching, and in this sense we have achieved a good compromise for CF-25-CPT material for a reasonable period followed by a quick unload of CPT-Suc and free CPT, which claims complete drug discharge within the target cells. In this context, an additional stability assay of CF-25-CPT in weakly acidic solution (PBS, 1x, pH=5.8) reported quick structure degradation due to boronate ester hydrolysis.

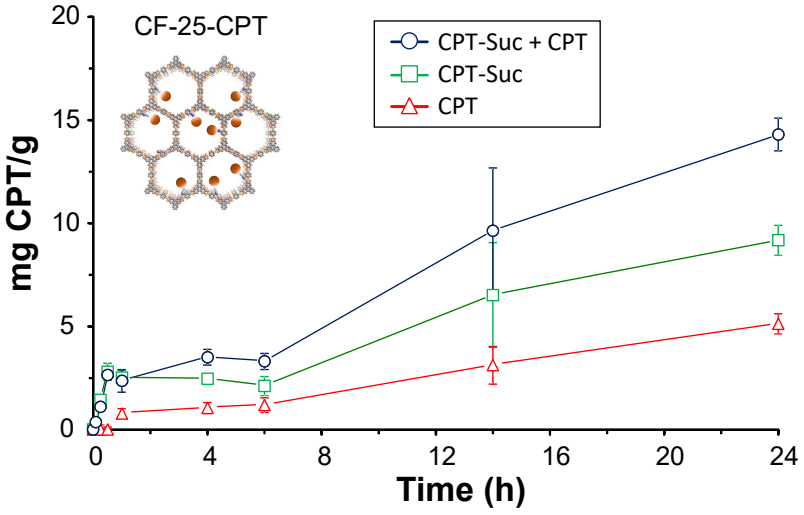

Fig. 6. Release kinetics of CPT in PBS at 37 °C. Conjugated (CPT-Suc) and free CPT are plotted, as well as the addition of both fractions (CPT-Suc + CPT = total CPT). All quantities are expressed as equivalent CPT.

Alternatively, the stability of CF-25-CPT nanoparticles was tested by incubating 1 mg/mL in DMEM medium at 37 ºC (supplemented with 10% FBS and 1% streptomycin/penicillin), observing a similar behavior pattern that in PBS (Fig. S16).

Conversely, CF-25/CPT platform prepared by physical adsorption (3% CPT wt/wt content) revealed very unstable in PBS, and released more than 80% of the therapeutic molecule in a few minutes due to almost instantaneous COF framework hydrolysis, and completed the process in less than 8 h (Fig. S17). This sample is not acceptable as DDS as it is unable to impose any controlled release over the drug, and no further biological validation was carried out.

Overall, CPT covalent incorporation in COF-5 channels provides additional resistance to hydrolytic digestion of the covalent organic framework, which is related to the partial pore blocking and hydrophobic profile associated to the high concentration of CPT molecules grafted.

3.4. Biological validation

As reported above, the novel CPT conjugate deploys the advisable requirements of stability in physiological fluids and no unspecific drug release is expected during the first hours after administration. Then, we performed a preliminary study of the biological activity by monitoring cell internalization and cytotoxicity of these materials over several human cancer cell lines.

Cell internalization studies were done over HeLa cell line with AF647 derivatives of CPT-25-CPT. This incorporated 1% of the fluorochrome with no significant changes in crystallinity. However, as the cytotoxic activity of CPT could strongly reduce living cells population, incubation time was shorten up to 6 hours, in order to avoid CPT incorporation to the cell cycle (CPT induces cell cycle arrest in G_2/M phase). Flow

cytometry results (Fig. 7a-c) showed particle cell internalization even at low concentration (1 μg mL^{-1}; 1.4%), that increased significantly at higher nanoparticle loading (5 μg mL^{-1}; 8.8%). No cell enlargement was observed (as expected for a DNA damaging agent like CPT), indicating that, even if nanoparticles carrying the drug are internalized, in these experimental conditions the drug is not able to get into nucleus and block the enzyme topoisomerase I. Actually, as already shown in different DDSs [53], hydrophobicity of CPT-loaded samples not only increases chemical stability against hydrolytic disruption, but also promotes interactions with the lipophilic cell membrane, which improves significantly cell internalization kinetics.

Additional cell uptake studies were performed by LCSM. HeLa cells were incubated for 6 hours with AF647-labelled CF-25-CPT (10 μg mL^{-1}), and the internalized nanoparticles were monitored by colocalization experiments. Cell were also stained with LysoTracker Green, a fluorescent probe used to label acidic organelles, and Hoechst 33342 for counterstaining of nuclei. Confocal microscope images (Fig. 7d-g) exhibit the AF647 fluorescence partially overlapped with the green fluorescesce of Lysotracker. These results, gathered with the FC study, indicate that CF-25 was able to transport and deliver CPT inside the cancer cells, probably via endocytosis, in a concentration-dependent manner.

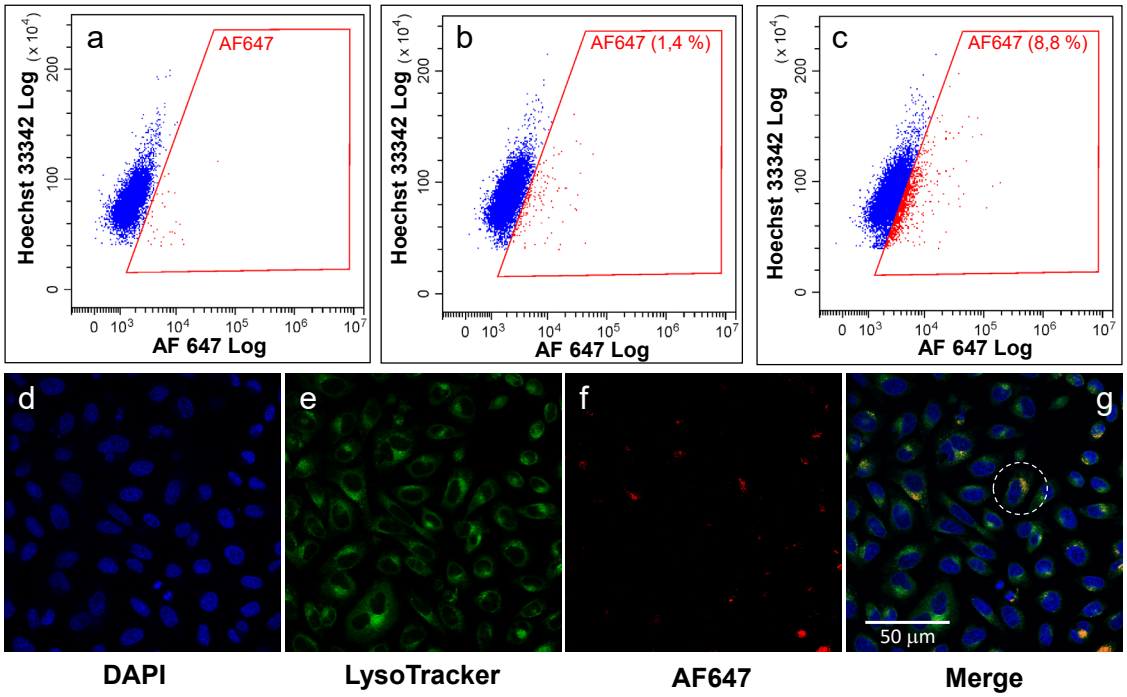

Fig. 7. Representative graphics of flow cytometry assays for HeLa cells incubated 6 h with 1 or 5 µg mL^{-1} of AF647 labeled CF-25-CPT and after DRAQ5 staining. Two-way plots were obtained and two different gated regions were quantified: cells with no nanoparticles (blue dots) and cells with nanoparticles (red dots). (a) Control of HeLa cells. (b) CF-25-CPT, 1 µg mL-1. (c) CF-25-CPT, 5 µg mL^{-1} Experiments were performed by using triplicate samples. Colocalization studies are presented for AF647 labeled CF-25-CPT at 10 µg mL^{-1} (d-g). Confocal images of the same Z-stacks were obtained for LysoTracker and AF647-conjugated nanoparticles, and merged to demonstrate that particles are allocated inside acidic compartments labeled by LysoTracker (dotted circle shows one example of colocalization region).

The biological activity of the novel CF-25-CPT conjugate was tested over HeLa and MCF-7 human cancer cell lines, calculating the corresponding half maximal inhibitory concentration (IC_{50}) values and comparing to the naked CPT molecule. Previously, non-loaded material lack of toxicity in the concentration range analyzed was assessed in a separated experiment, showing that even at the highest particle loading, the relative cell viability was above 80%, corresponding to an acceptable biocompatibility profile [54]. The results (Fig. 8) show that CF-25-CPT is always more active than the free drug, irrespectively of the cancer cell line, with IC_{50} values clearly lower than CPT (Table 2).

This is consistent with the promoted cell internalization of nanoparticles observed by flow cytometry. Here, drug discharge is expected to take place quickly inside cells, as boronate ester-linked polymers are quickly hydrolyzed under acid pH at lysosomes, releasing completely their therapeutic load. To confirm the role of CF-25 as CPT safe vehicle into cancer cells in our experimental conditions we carried out control experiments by incubating HeLa or MCF-7 cells with CF-25 and CPT at the same well, obtaining lower cytotoxic activity than for the conjugate CF-25-CPT, with IC_{50} values close to that of the naked drug.

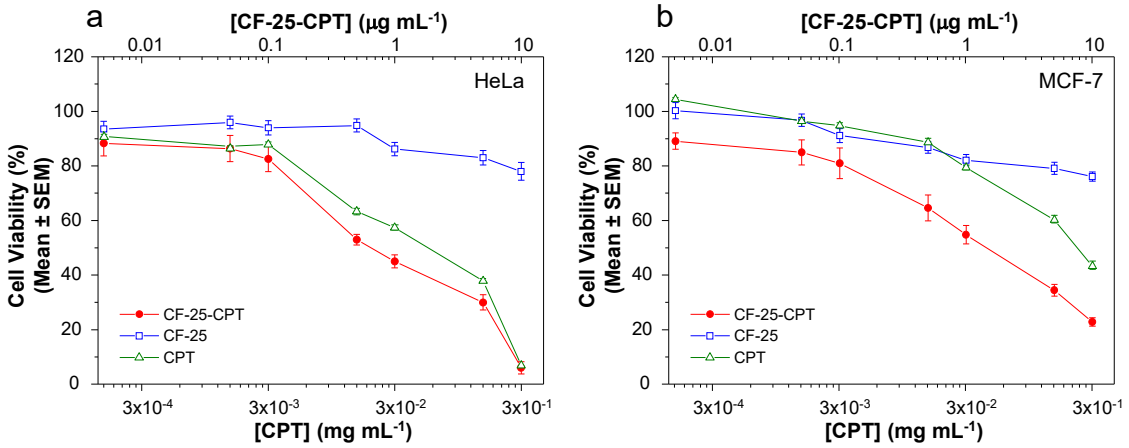

Fig. 8. MTT cell viability assays in HeLa (d) and MCF-7 (e) cell lines. Sample concentration is referred to CPT equivalent (lower scale). Non-loaded material (CF-25) was also tested over every cell line, and its concentration is referred at the upper scale. Cell viability data are expressed as mean ± SEM (n = 3).

Table 2

IC_{50} values of CPT and different CPT/CF-25 combinations obtained over HeLa and MCF-7 cell lines.[a]

Cell line	CPT	CF-25-CPT	CPT + CF-25[b]
HeLa	0.044 ± 0.005	0.020 ± 0.002	0.031 ± 0.004
MCF-7	0.053 ± 0.009	0.034 ± 0.005	0.044 ± 0.005

[a] Each value indicates the mean ± SEM (µg/mL). All the experiments were carried out in triplicate.

[b] CPT + CF-25 = control experiments by incubating cells with CF-25 particles and CPT in the same well.

Finally, even if we have not introduced any targeting molecule in this nanoplatform to target selectively the cancer cells, we can consider some specificity in its cytotoxic action due to the differences in the biological cycle of malign cells, and their superior cell doubling time associated to their stressed metabolism. For instance, in the case of HeLa, the doubling time is 23 h, whereas in the case of fibroblasts is higher than 45 h [55]. In order to confirm this, we carried out a cell viability assay over mouse L929 fibroblast cell line with CF-25-CPT and free CPT, and the results are shown in Fig. S18 at the Supplementary Data. When comparing these results with those of Table 2, it is noticeable that CPT and CF-25-CPT are less cytotoxic over fibroblasts, with half maximal inhibitory concentration (IC_{50}) over two fold in case of CF-25-CPT. In case of the free drug it was not possible to calculate the IC_{50} value as the cell viability did not go below 50% in the studied range of concentrations. This is not surprising, as the cytotoxic effect of CPT is based in the inhibition of topoisomerase I during mitosis, and the lower growth rate of the L929 cell line minimizes the activity of the drug.

4. Conclusions

We have shown that pore wall functionalization in a covalent organic framework (COF-5) with a nucleophyllic group (NH_2) is possible through a direct (one-pot) synthetic protocol by serial substitution of original monomers up to 60%. Above this limit the mesoporous structure collapses.

The obtained functionality in the as-synthesized material allows subsequent post-synthetic modification steps, and this model has allowed us to prepare a novel type of drug delivery system based on covalent linking of a therapeutic molecule in COF structure, by coupling of camptothecin-20-*O*-hemisuccinate (CPT-Suc) over primary amino functions. The resulting conjugate presents neither significant alteration of the π–π

stacking model (AA) nor changes of structure lattice parameter, although it suffers a dramatic reductions of porosity due to strong pore blocking.

Water adsorption isotherms modelling anticipate that the insertion of CPT ligand in the framework promotes an acute hydrophobic effect that protects a region of COF chain from boronate ester hydrolysis and resulting degradation. This is confirmed by monitoring structure stability in aqueous medium, resulting in an additional resistance of the CPT-substituted material to hydrolytic digestion, due to partial pore blocking and hydrophilic profile associated to the high concentration of drug molecules grafted.

The modified nanoCOF is effectively internalized in cells and performs higher cytotoxic activity than the free drug, which is consistent with the strengthened stability and promoted interactions of the hydrophobic particles with the lipophilic cell membrane, improving significantly cell uptake kinetics.

Overall, this novel CPT nanoplatform based in amino derivatized COF-5 material is able to offer a modulated biological response, providing high cytotoxic activity even at low dose, and stimuli-responsive intracellular drug release. The potential bioavailability is also excellent, as their basic components (e.g., structural ligands) are expected to be fully eliminated in living organisms by renal filtration, avoiding any side accumulation in tissues. We are currently expanding this model to different COF structures, introducing variable functionalities and drugs.

Declaration of competing interest

The authors declare no competing interest.

Acknowledgements

Financial support of the Spanish Ministry of Economy and Competitiveness (projects TEC2016-80976-R and SEV-2016-0683) is gratefully acknowledged. A.S.O. thanks the

PDSE Scholarship supported by CAPES/Brazil. A.M. thanks Generalitat Valenciana for a predoctoral fellowship GRISOLIAP/2019/084. We fully appreciate the assistance of the ASIC computational facilities and the Electron Microscopy Service of the Universitat Politècnica de València.

Supplementary data

Supplementary Information available: General methods; synthetic protocols; powder XRD patterns; N_2 adsorption-desorption isotherms; ^{1}H-NMR compositional analysis; optimized structures simulations; water adsorption isotherms modelling; Young modulus modelling; ^{1}H-NMR spectra in water; stability in physiological medium.

References

[1] P.J. Waller, F. Gándara, O.M. Yaghi, Chemistry of Covalent Organic Frameworks, Acc. Chem. Res. 48 (2015) 3053–3063. doi:10.1021/acs.accounts.5b00369.

[2] H. Furukawa, O.M. Yaghi, Storage of Hydrogen, Methane, and Carbon Dioxide in Highly Porous Covalent Organic Frameworks for Clean Energy Applications, J. Am. Chem. Soc. 131 (2009) 8875–8883. doi:10.1021/ja9015765.

[3] H. Oh, S.B. Kalidindi, Y. Um, S. Bureekaew, R. Schmid, R.A. Fischer, M. Hirscher, A cryogenically flexible covalent organic framework for efficient hydrogen isotope separation by quantum sieving, Angew. Chemie - Int. Ed. 52 (2013) 13219–13222. doi:10.1002/anie.201307443.

[4] S.Y. Ding, J. Gao, Q. Wang, Y. Zhang, W.G. Song, C.Y. Su, W. Wang, Construction of covalent organic framework for catalysis: Pd/COF-LZU1 in Suzuki-Miyaura coupling reaction, J. Am. Chem. Soc. 133 (2011) 19816–19822. doi:10.1021/ja206846p.

[5] S. Chandra, T. Kundu, S. Kandambeth, R. Babarao, Y. Marathe, S.M. Kunjir, R. Banerjee, Phosphoric acid loaded azo (-N=N-) based covalent organic framework for proton conduction, J. Am. Chem. Soc. 136 (2014) 6570–6573. doi:10.1021/ja502212v.

[6] C.R. Deblase, K.E. Silberstein, T.T. Truong, H.D. Abruña, W.R. Dichtel, B-Ketoenamine-Linked Covalent Organic Frameworks Capable of Pseudocapacitive Energy Storage, J. Am. Chem. Soc. 135 (2013) 16821–16824. doi:10.1021/ja409421d.

[7] Q. Gao, X. Li, G.H. Ning, H. Sen Xu, C. Liu, B. Tian, W. Tang, K.P. Loh,

Covalent Organic Framework with Frustrated Bonding Network for Enhanced Carbon Dioxide Storage, Chem. Mater. 30 (2018) 1762–1768. doi:10.1021/acs.chemmater.8b00117.

[8] J.L. Segura, S. Rayuela, M.M. Ramos, Post-synthetic modification of covalent organic frameworks, Chem. Soc. Rev. 48 (2019) 3903–3945. doi:10.1039/c8cs00978c.

[9] J.L. Sainan Liu, Chunling Hu, Ying Liu, Xueyan Zhao, Maolin Pang, One-Pot Synthesis of DOX@Covalent Organic Framework with Enhanced Chemotherapeutic Efficacy, Chem Eur J. 25 (2019) 4315–4319. doi:10.1002/chem.201806242.

[10] G. Zhang, X. Li, Q. Liao, Y. Liu, K. Xi, W. Huang, X. Jia, Water-dispersible PEG-curcumin/amine-functionalized covalent organic framework nanocomposites as smart carriers for in vivo drug delivery, Nat. Commun. 9 (2018) 1–11. doi:10.1038/s41467-018-04910-5.

[11] Q. Guan, D.D. Fu, Y.A. Li, X.M. Kong, Z.Y. Wei, W.Y. Li, S.J. Zhang, Y. Bin Dong, BODIPY-Decorated Nanoscale Covalent Organic Frameworks for Photodynamic Therapy, IScience. 14 (2019) 180–198. doi:10.1016/j.isci.2019.03.028.

[12] E.L. Spliter, W.R. Dichtel, Lewis acid-catalysed formation of two-dimensional phthalocyanine covalent organic frameworks, Nat. Chem. 2 (2010) 672–677.

[13] H. Li, A.D. Chavez, H. Li, H. Li, W.R. Dichtel, J.L. Bredas, Nucleation and Growth of Covalent Organic Frameworks from Solution: The Example of COF-5, J. Am. Chem. Soc. 139 (2017) 16310–16318. doi:10.1021/jacs.7b09169.

[14] D.N. Bunck, W.R. Dichtel, Internal functionalization of three-dimensional

covalent organic frameworks, Angew. Chemie - Int. Ed. 51 (2012) 1885–1889. doi:10.1002/anie.201108462.

[15] S.D. Brucks, D.N. Bunck, W.R. Dichtel, Functionalization of 3D covalent organic frameworks using monofunctional boronic acids, Polym. (United Kingdom) 55 (2014) 330–334. doi:10.1016/j.polymer.2013.07.030.

[16] A. Nagai, Z. Guo, X. Feng, S. Jin, X. Chen, X. Ding, D. Jiang, Pore surface engineering in covalent organic frameworks, Nat. Commun. 2 (2011) 536–538. doi:10.1038/ncomms1542.

[17] D.N. Bunck, W.R. Dichtel, Postsynthetic functionalization of 3D covalent organic frameworks, Chem. Commun. 49 (2013) 2457. doi:10.1039/c3cc40358k.

[18] N. Huang, R. Krishna, D. Jiang, Tailor-Made Pore Surface Engineering in Covalent Organic Frameworks: Systematic Functionalization for Performance Screening, J. Am. Chem. Soc. 137 (2015) 7079–7082. doi:10.1021/jacs.5b04300.

[19] M.S. Lohse, T. Stassin, G. Naudin, S. Wuttke, R. Ameloot, D. De Vos, D.D. Medina, T. Bein, Sequential Pore Wall Modification in a Covalent Organic Framework for Application in Lactic Acid Adsorption, Chem. Mater. 28 (2016) 626–631. doi:10.1021/acs.chemmater.5b04388.

[20] M. Calik, T. Sick, M. Dogru, M. Döblinger, S. Datz, H. Budde, A. Hartschuh, F. Auras, T. Bein, From Highly Crystalline to Outer Surface-Functionalized Covalent Organic Frameworks-A Modulation Approach, J. Am. Chem. Soc. 138 (2016) 1234–1239. doi:10.1021/jacs.5b10708.

[21] A.P. Cote, A.I. Benin, N.W. Ockwig, M. O'Keeffe, A.J. Maatzger, O.M. Yaghi, Porous, Crystalline, Covalent Organic Frameworks, Science 310 (2005) 1166–1170. doi:10.1126/science.1120411.

[22] M.L. Stolowitz, E.A. Kesicki, K.P. Lund, K.A. Hughes, Phenyldiboronic acid reagents and complexes, US Patent 6075126, 2000.

[23] S. Norbedo, F. Dinon, M. Bergamin, S. Bosi, V. Aroulmoji, R. Khan, E. Murano, Synthesis of 6-amino-6-deoxyhyaluronan as an intermediate for conjugation with carboxylate-containing compounds: application to hyaluronan-camptothecin conjugates, Carbohydr. Res. 344 (2009) 98–104. doi:10.1016/j.carres.2008.09.027.

[24] O. Koniev, A. Wagner, Developments and recent advancements in the field of endogenous amino acid selective bond forming reactions for bioconjugation, Chem. Soc. Rev. 44 (2015) 5495–5551. doi:10.1039/c5cs00048c.

[25] O. Yahiaoui, A.N. Fitch, F. Hoffmann, M. Fröba, A. Thomas, J. Roeser, 3D anionic silicate covalent organic framework with srs topology, J. Am. Chem. Soc. 140 (2018) 5330–5333. doi:10.1021/jacs.8b01774.

[26] A.K. Rappé, C.J. Casewit, K.S. Colwell, W.A. Goddard, W.M. Skiff, UFF, a Full Periodic Table Force Field for Molecular Mechanics and Molecular Dynamics Simulations, J. Am. Chem. Soc. 114 (1992) 10024–10035. doi:10.1021/ja00051a040.

[27] J.D. Gale, GULP: A computer program for the symmetry-adapted simulation of solids, J. Chem. Soc., Faraday Trans. 93 (1997) 629–637. doi:10.1039/A606455H.

[28] D. Dubbeldam, S. Calero, D.E. Ellis, R.Q. Snurr, RASPA: Molecular simulation software for adsorption and diffusion in flexible nanoporous materials, Mol. Simul. 42 (2016) 81–101. doi:10.1080/08927022.2015.1010082.

[29] H.J.C. Berendsen, J.R. Grigera, T.P. Straatsma, The Missing Term in Effective

Pair Potentials1, J. Phys. Chem. 91 (1987) 6269–6271. doi:10.1021/j100308a038.

[30] P. Mark, L. Nilsson, Structure and Dynamics of the TIP3P, SPC, and SPC / E Water Models at 298 K, J. Phys. Chem. A. 105 (2001) 9954–9960. doi:10.1021/jp003020w.

[31] C. Adamo, V. Barone, Toward reliable density functional methods without adjustable parameters: The PBE0 model, J. Chem. Phys. 110 (1999) 6158–6170. doi:10.1063/1.478522.

[32] M. J. Frisch, G.W. Trucks, H.B. Schlegel, G.E. Scuseria, M.A. Robb, J.R. Cheeseman, G. Scalmani, V. Barone, B. Mennucci, G.A. Petersson, H. Nakatsuji, M. Caricato, X. Li, H.P. Hratchian, A.F. Izmaylov, J. Bloino, J. G. Zheng, J. L. Sonnenberg, M. Hada, M. Ehara, K. Toyota, R. Fukuda, J. Hasegawa, M. Ishida, T. Nakajima, Y. Honda, O. Kitao, H. Nakai, T. Vreven, J. A. Montgomery, J.E. Peralta, F. Ogliaro, M. Bearpark, J.J. Heyd, E. Brothers, K.N. Kudin, V.N. Staroverov, R. Kobayashi, J. Normand, K. Raghavachari, A. Rendell, J.C. Burant, S.S. Iyengar, J. Tomasi, M. Cossi, N. Rega, J.M. Millam, M. Klene, J.E. Knox, J.B. Cross, V. Bakken, C. Adamo, J. Jaramillo, A.D. R. Gomperts, R. E. Stratmann, O. Yazyev, A. J. Austin, R. Cammi, C. Pomelli, J. W. Ochterski, R. L. Martin, K. Morokuma, V. G. Zakrzewski, G. A. Voth, P. Salvador, J. J. Dannenberg, S. Dapprich, A.D. Daniels, O. Farkas, J.B. Foresman, J. V. Ortiz, J. Cioslowski, D.J. Fox, Gaussian 09, Revision A.02, Gaussian, Inc., Wallingford CT, 2009.

[33] D.S. Otkidach, I. V. Pletnev, Conformational analysis of boron-containing compounds using Gillespie - Kepert version of molecular mechanics, J. Mol. Struct. THEOCHEM. 536 (2001) 65–72. doi:10.1016/S0166-1280(00)00602-3.

[34] A. Tafi, M. Agamennone, P. Tortorella, S. Alcaro, C. Gallina, M. Botta, AMBER force field implementation of the boronate function to simulate the inhibition of β-lactamases by alkyl and aryl boronic acids, Eur. J. Med. Chem. 40 (2005) 1134–1142. doi:10.1016/j.ejmech.2005.06.011.

[35] L.M. Lanni, R.W. Tilford, M. Bharathy, J.J. Lavigne, Enhanced hydrolytic stability of self-assembling alkylated two-dimensional covalent organic frameworks, J. Am. Chem. Soc. 133 (2011) 13975–13983. doi:10.1021/ja203807h.

[36] Y. Du, K. Mao, P. Kamakoti, P. Ravikovitch, C. Paur, S. Cundy, Q. Li, D. Calabro, Experimental and computational studies of pyridine-assisted post-synthesis modified air stable covalent–organic frameworks, Chem. Commun. 48 (2012) 4606. doi:10.1039/c2cc30781b.

[37] B.J. Smith, N. Hwang, A.D. Chavez, J.L. Novotney, W.R. Dichtel, Growth rates and water stability of 2D boronate ester covalent organic frameworks, Chem. Commun. 51 (2015) 7532–7535. doi:10.1039/C5CC00379B.

[38] Q. Fang, J. Wang, S. Gu, R.B. Kaspar, Z. Zhuang, J. Zheng, H. Guo, S. Qiu, Y. Yan, 3D Porous Crystalline Polyimide Covalent Organic Frameworks for Drug Delivery, J. Am. Chem. Soc. 137 (2015) 8352–8355. doi:10.1021/jacs.5b04147.

[39] L. Bai, S.Z.F. Phua, W.Q. Lim, A. Jana, Z. Luo, H.P. Tham, L. Zhao, Q. Gao, Y. Zhao, Nanoscale covalent organic frameworks as smart carriers for drug delivery, Chem. Commun. 52 (2016) 4128–4131. doi:10.1039/C6CC00853D.

[40] S. Mitra, H.S. Sasmal, T. Kundu, S. Kandambeth, K. Illath, D. Díaz Díaz, R. Banerjee, Targeted Drug Delivery in Covalent Organic Nanosheets (CONs) via Sequential Postsynthetic Modification, J. Am. Chem. Soc. 139 (2017) 4513–

4520. doi:10.1021/jacs.7b00925.

[41] P. Bhanja, S. Mishra, K. Manna, A. Mallick, K. Das Saha, A. Bhaumik, Covalent Organic Framework Material Bearing Phloroglucinol Building Units as a Potent Anticancer Agent, ACS Appl. Mater. Interfaces. 9 (2017) 31411–31423. doi:10.1021/acsami.7b07343.

[42] B. Lukose, A. Kuc, T. Heine, The structure of layered covalent-organic frameworks, Chem. - A Eur. J. 17 (2011) 2388–2392. doi:10.1002/chem.201001290.

[43] Z.F. Pang, T.Y. Zhou, R.R. Liang, Q.Y. Qi, X. Zhao, Regulating the topology of 2D covalent organic frameworks by the rational introduction of substituents, Chem. Sci. 8 (2017) 3866–3870. doi:10.1039/c6sc05673c.

[44] X. Wu, X. Han, Y. Liu, Y. Liu, Y. Cui, Control Interlayer Stacking and Chemical Stability of Two-Dimensional Covalent Organic Frameworks via Steric Tuning, J. Am. Chem. Soc. 140 (2018) 16124–16133. doi:10.1021/jacs.8b08452.

[45] N. Sanna, G. Chillemi, L. Gontrani, A. Grandi, G. Mancini, S. Castelli, G. Zagotto, C. Zazza, V. Barone, A. Desideri, UV-vis spectra of the anticancer campothecin family drugs in aqueous solution: Specific spectroscopic signatures unraveled by a combined computational and experimental study, J. Phys. Chem. B. 113 (2009) 5369–5375. doi:10.1021/jp809801y.

[46] J. Dey, I.M. Warner, Spectroscopic and photophysical studies of the anticancer drug: Camptothecin, J. Luminiscence 71 (1997) 105–114. doi:10.1016/S0022-2313(96)00125-1.

[47] S.J. Kaldas, T. Rogova, V.G. Nenajdenko, A.K. Yudin, Modular Synthesis of β -Amino Boronate Peptidomimetics, J. Org. Chem. 83 (2018) 7296–7302.

doi:10.1021/acs.joc.8b00325.

[48] D.G. Hall, Boronic acid catalysis, Chem Soc Rev. 48 (2019) 3475–3496. doi:10.1039/C9CS00191C.

[49] P. Botella, E. Rivero-Buceta, Safe approaches for camptothecin delivery: Structural analogues and nanomedicines, J. Control. Release. 247 (2017) 28–54. doi:10.1016/j.jconrel.2016.12.023.

[50] P. Botella, I. Abasolo, Y. Fernández, C. Muniesa, S. Miranda, M. Quesada, J. Ruiz, S. Schwartz, A. Corma, Surface-modified silica nanoparticles for tumor-targeted delivery of camptothecin and its biological evaluation, J. Control. Release. 156 (2011) 246–257. doi:10.1016/j.jconrel.2011.06.039.

[51] A. Cabrera-garcía, E. Checa-chavarria, E. Rivero-buceta, V. Moreno, E. Fernández, P. Botella, Journal of Colloid and Interface Science Amino modified metal-organic frameworks as pH-responsive nanoplatforms for safe delivery of camptothecin, 541 (2019) 163–174. doi:10.1016/j.jcis.2019.01.042.

[52] J. Cheng, K.T. Khin, G.S. Jensen, A. Liu, M.E. Davis, Synthesis of linear, β-cyclodextrin-based polymers and their camptothecin conjugates, Bioconjug. Chem. 14 (2003) 1007–1017. doi:10.1021/bc0340924.

[53] P. Botella, C. Muniesa, V. Vicente, A. Cabrera-García, Effect of drug precursor in cell uptake and cytotoxicity of redox-responsive camptothecin nanomedicines, Mater. Sci. Eng. C. 58 (2016) 692–699. doi:10.1016/j.msec.2015.09.012.

[54] T.L. Riss, R.A. Moravec, A.L. Niles, S. Duellman, H.A. Benink, T.J. Worzella, L. Minor, Cell Viability Assays, in: Assay Guid. Man., 2013: pp. 785–796. doi:10.1016/j.acthis.2012.01.006.

[55] V. Moulin, D. Mayrand, A. Laforce-Lavoie, S. Larochelle, H. Genest, In Vitro

Culture Methods of Skin Cells for Optimal Skin Reconstruction by Tissue Engineering, in: D. Eberli (Ed.), Regen. Med. Tissue Eng. - Cells Biomater., InTech, Rijeka, 2011: pp. 195–208. doi:10.5772/20341.

Graphical Abstract